SEISMIC RISK ASSESSMENT AT URBAN SCALE FROM 3D PHYSICS-BASED NUMERICAL MODELING: THE CASE OF THESSALONIKI

by

Chiara SMERZINI[1] and Kyriazis PITILAKIS[2]

[1] Department of Civil and Environmental Engineering, Politecnico di Milano, Piazza Leonardo da Vinci 32, 20133 Milano, Italy
[2]Aristotle University, Department of Civil Engineering, Research Unit of Geotechnical Earthquake Engineering and Soil Dynamics, P.O.B 424, 54124 Thessaloniki, Greece

Corresponding author

Chiara Smerzini

Department of Civil and Environmental Engineering, Politecnico di Milano.

Email: chiara.smerzini@polimi.it.

Tel.: +39 0223996283

ABSTRACT

The main aim of this work is to present a prototype of seismic risk assessment study at urban scale which incorporates next generation tools for hazard assessment, with application to the city of Thessaloniki, Northern Greece. The key ingredient of the proposed approach is the characterization of earthquake ground motion by means of three-dimensional broadband physics-based numerical simulations, which explicitly account for the fault rupture, the propagation path in heterogeneous media and complex geological conditions. The seismic damage of contemporary reinforced concrete building stock of the city of Thessaloniki has been evaluated using the capacity spectrum method, for a scenario corresponding to the destructive historical earthquake of June 20th 1978 (M_W6.5). Although the vulnerability model considered in these analyses reflects the contemporary building stock and, hence, differs from the situation at the time of the earthquake, the soundness of our damage estimates has been successfully verified through the comparison with the post-1978 earthquake damage observations. Results of this study demonstrate that 3D physics-based simulations can provide a more accurate and detailed characterization of earthquake ground motion and of its spatial variability, as compared to standard empirical approaches, and can be effectively used to improve seismic risk studies for strategic urban areas.

Keywords: seismic risk; capacity spectrum method; 3D physics-based numerical modeling; displacement-based fragility functions

1. INTRODUCTION

Seismic risk studies at urban scale are crucial: (i) to assess quantitatively the socio-economic impact of future earthquakes on a densely populated area, of potential interest for insurance and reinsurance industries; (ii) to assist national authorities in planning effective actions for seismic risk mitigation and preparedness, including also the drafting of seismic codes for the design of new structures; (iii) to improve decision making in support to emergency response and disaster management; and eventually (iv) to optimize retrofitting strategies. The seminal goal of such studies is to estimate the spatial distribution of the expected damages and losses to structures and people due to an earthquake of any intensity. Key ingredients to achieve this goal are, on one hand, the accurate evaluation of seismic hazard and of its spatial variability, and, on the other one, the use of up-to-date vulnerability models, which establish a correlation between hazard and structural damage.

Standard methods for hazard assessment, both in a probabilistic and deterministic framework, are based on the use of Ground Motion Prediction Equations (GMPEs), which are empirical regression laws for peak ground motion parameters calibrated on instrumental observations from past earthquakes. In spite of their simplicity and their enormous progress in recent years, they have some intrinsic drawbacks, especially when applied to the evaluation of seismic risk at regional scale. Specifically, (1) they are poorly constrained in the conditions of potential major interest for seismic risk reduction objectives, in particular, in the near-source region of large, destructive earthquakes; (2) characterization of site condition, typically parametrized in terms of shear wave velocity in the top 30 m (V_{S30}), may not be fully adequate to describe complex site effects at local scale, such as those occurring in alluvial valleys where densely populated urban centers are often built; (3) they provide only estimates of peak ground motion, without the entire waveform, of potential interest for non-linear time history analyses of structures; (4) they cannot provide an accurate description of the spatial correlation between peak ground motion intensities at multiple sites. Referring to the latter point, it is widely recognized that a proper description of the spatial variability of ground motion intensity is of paramount importance for seismic risk and loss assessment of large urban areas with spatially distributed building portfolios and infrastructure systems (see e.g. Park et al. 2007; Jayaram and Baker 2010; Weatherill et al. 2015). For this reason, in such cases,

69 additional models describing the spatial correlation structure of ground motion have to be
70 implemented (see e.g. Jayaram and Baker 2009; Esposito and Iervolino 2011; 2012), in
71 conjunction with GMPEs.

72 To overcome these limitations, three-dimensional (3D) physics-based numerical simulation of
73 earthquake ground motion has emerged as a powerful alternative tool to the use of GMPEs.
74 Based on the rigorous numerical solution of the elastodynamics equation, simulations provide
75 synthetic ground motion time histories reflecting the physics of the seismic wave propagation
76 problem from the source up to the site of interest, including directivity effects in near fault
77 conditions, topographic and complex site effects. Although its use remains rather limited in
78 engineering practice, such an approach has become feasible and mature enough owing to the
79 continuous progress of computational resources and to the increasing number of verification
80 experiments (see e.g. Bielak et al. 2010; Chaljub et al. 2010; SCEC project:
81 https://www.scec.org/workshops/2016/gmsv) and validation studies against real recordings
82 (Taborda and Bielak 2014; Paolucci et al. 2015; Gallovič 2016).

83 Among the state-of-the-art methodologies for vulnerability assessment (for a thorough review
84 see Calvi et al. 2006), those based on the Capacity Spectrum Method, referred to hereafter as
85 CSM (Freeman 2004), are recommended in the HAZUS procedure (FEMA 1999) and ATC-
86 40 (ATC 1996). The CSM is a performance-based method which provides the estimate of the
87 median response of an idealized non-linear single degree of freedom oscillator, when
88 subjected to a postulated ground shaking scenario, at the performance point of the structure.
89 The latter is determined graphically as the intersection between the capacity of the structure,
90 in the form of a pushover curve, with the seismic demand, in the response spectral
91 displacement and acceleration space. This approach has been applied successfully for seismic
92 risk evaluation in different urban environments worldwide (Erdik et al. 2003; Barbat et al.
93 2008; Riga et al. 2017) and this will be the method used in this paper.

94 The main aim of this paper is to present a novel approach for scenario-based seismic risk
95 assessment study at urban scale, incorporating next generation tools for the hazard evaluation,
96 based on physics-based numerical simulations of ground shaking including an explicit 3D
97 model of the seismic source, the propagation path and geological basin structures. There are
98 very few case studies in the literature where 3D physics-based numerical simulations have
99 been included in the methodological chain for seismic risk assessment. To the authors'

knowledge, the Great Southern California Shake-Out Project (Porter et al. 2011) has been the only study so far using 3D physics-based numerical simulations to estimate the large-scale physical damage of built environment as well as the economic losses caused by a hypothetical major earthquake (M 7.8) in Southern California.

In this work, the city of Thessaloniki, Northern Greece, is taken as case study owing to the abundance of detailed data regarding both the local geology and the exposed building stock. Recent works (Pitilakis et al. 2015; Riga et al. 2017) have addressed the seismic risk assessment in the city of Thessaloniki using the CSM but in these studies a different representation of seismic hazard was adopted, based on the available PSHA studies combined with either code-based or detailed soil classification schemes and site specific ground response analyses. In this study a step forward will be made by incorporating the results of a 3D physics-based scenario reproducing with reasonable accuracy the historical Volvi earthquake of June 20th 1978 (moment magnitude M_W=6.5), which affected dramatically the city of Thessaloniki.

For this purpose, starting from the numerical analyses performed by Smerzini et al. (2017), reliable only in a limited frequency range, specifically up to about 1.5 Hz, a promising approach based on Artificial Neural Networks has been applied to enrich the frequency content of the synthetic ground motions and, therefore, make them usable for the evaluation of the damage for the contemporary Reinforced Concrete (RC) building stock. Maps of expected damage for the RC building portfolio in the urban area of Thessaloniki will be produced and compared with actual damage observations to highlight the feasibility and advantages of using 3D physics-based numerical simulations in risk analyses at urban scale.

2. STUDY AREA

The study area is located in one of the most seismo-tectonically active zones in Europe. Its seismicity is mainly associated with the activity of the Mygdonia and the Anthemountas fault systems, which were responsible of severe destructive earthquakes with magnitude up to 7 from historical times to present (Papazachos and Papazachou 1997). Thessaloniki, the second largest city in Greece after Athens, is the financial center in Northern Greece and was the first modern urban center in Greece hit by a major earthquake. The M_W 6.5 June 20th 1978

129 earthquake occurred near the Volvi and Langada lakes, at nearly 30 km to the East of the city
130 of Thessaloniki, and had a tremendous impact on the city, causing 47 victims, most of them in
131 an eight-storey RC building which collapsed, 220 injuries and serious damages to about 4000
132 buildings (Penelis et al. 1988; Panou et al. 2014). The earthquake revealed indeed the extreme
133 fragility of a modern society where a significant portion of the building stock was constructed
134 in RC including basic earthquake-resistant design criteria (post 1959 code). The extensive
135 damage induced by the 1978 event encouraged the development of a series of research studies
136 aimed at improving the knowledge on the seismotectonic context (see overview in Roumelioti
137 et al. 2007), at providing a large-scale geophysical and geotechnical characterization for
138 microzonation purposes (e.g.,. Anastasiadis et al. 2001; Apostolidis et al. 2004), as well as at
139 defining detailed vulnerability and exposure models for contemporary and masonry buildings,
140 lifeline and utility systems (see e.g. Kappos et al. 2006; Argyroudis et al. 2014).

141 Figure 1 shows the study area on two scales: on the broader scale used for seismic hazard
142 assessment through 3D numerical modeling (bottom) and on the scale of the central
143 municipality of the city of Thessaloniki considered for risk assessment (top). The latter is
144 subdivided into twenty Sub-City Districts (SCD), based on the European Urban Audit
145 database provided by EUROSTAT (http://www. urbanaudit.org), and has a total population of
146 about 380,000 inhabitants, corresponding roughly to one third of the population in the whole
147 urban agglomerate.

148 In this work seismic risk will be evaluated only for the contemporary RC building stock, as it
149 constitutes the majority of the buildings in the study area. The building inventory was
150 compiled in previous studies, first, within the 2001-2004 RISK-UE Project (Pitilakis et al.
151 2004) and, then, within the 2009-2012 Syner-G Project (Pitilakis et al. 2014), and has been
152 used in recent seismic risk studies (Kappos et al. 2008; Riga et al. 2017; Pitilakis et al. 2015).
153 The elementary unit of the building inventory is the building block (BDG), which comprises
154 the buildings included in a 50 m wide rectangular area. The inventory includes 2892 building
155 blocks, classified into 54 different building typologies according to the Building Typologies
156 Matrix (BTM) classification scheme proposed by Kappos et al. (2006), as reported in Table 1.

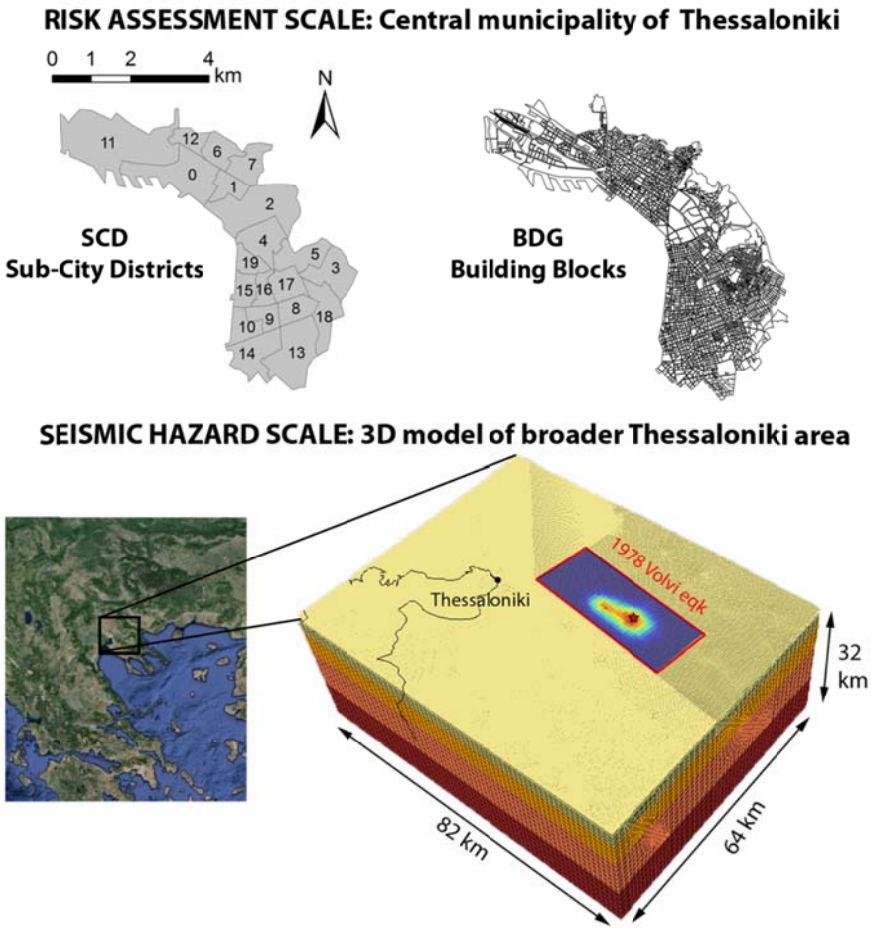

Figure 1 Study area, from the seismic hazard scale of 3D numerical modeling (bottom) to the risk assessment scale of the central municipality of the city of Thessaloniki (top) consisting of 20 sub-city districts, SCD (left), and 2892 building blocks BDG (right).

The BTM is suitable to describe practically all common RC building types present in Greece and is based on a rigorous classification of the buildings as follows:

(a) structural system: RC1= Concrete moment frames; RC3 = Concrete frames with unreinforced masonry infill walls and; RC4 = RC Dual systems. RC3 and RC4 buildings are further classified depending on the configuration of infill walls;

(b) height: low (L: 1-3 storeys), medium (M: 4-7 storeys) and high (H: ≥8 storeys) rise buildings;

(c) level of seismic design: N = No code (or pre-code), representing RC buildings with very low level of seismic design or no seismic design at all, and poor quality of detailing of critical elements; L = Low code, denoting RC buildings with low level of

seismic design (roughly corresponding to pre-1980 codes in S. Europe, e.g., the 1959 Code for Greece); M = Moderate code, representing RC buildings with medium level of seismic design (roughly corresponding to post-1980 codes in S. Europe, e.g., the 1985 Supplementary Clauses of the Greek Seismic Codes) and reasonable seismic detailing of R/C members; H = High code, representing RC buildings with enhanced level of seismic design and ductile seismic detailing of R/C members according to the new generation of seismic codes (similar to Eurocode 8, CEN 2004).

Each building typology is hence referred to with the following acronym RCS.XHC, where S.X represents the structural system, H the height and C the code class.

Figure 2 shows the classification of the Thessaloniki buildings based on structural system (a), height (b), code level (c) and building type (d) according to the BTM of Table 1. The majority of buildings belongs to the RC4.2ML (about 33%) and RC4.3ML (21%) classes, i.e., medium-rise RC buildings with regularly and irregularly infilled dual systems and low code level prior to 1980, with minor contributions from RC4.2MM (7.7%), RC4.3HL (8%), and RC4.3MM (8%) classes.

Table 1 RC Building Typology Matrix (BTM) for the city of Thessaloniki city (from Kappos et al. 2006).

Type	Structural system	Height	Code level
RC1	Concrete moment frames	(L) Low-rise (1-3) (M) Mid-rise (4-7) (H) High-rise (8+)	(N)o/pre code (L)ow code (M)edium code (H)igh code
RC3	Concrete frames with unreinforced masonry infill walls		
3.1	Regularly infilled frames	(L) Low-rise (1-3) (M) Mid-rise (4-7) (H) High-rise (8+)	(N)o/pre code (L)ow code (M)edium code (H)igh code
3.2	Irregularly infilled frames (pilotis)	(L) Low-rise (1-3) (M) Mid-rise (4-7) (H) High-rise (8+)	(N)o/pre code (L)ow code (M)edium code (H)igh code
RC4	RC Dual systems (RC frames and walls)		
4.1	Bare Systems (no infill walls)	(L) Low-rise (1-3) (M) Mid-rise (4-7) (H) High-rise (8+)	(N)o/pre code (L)ow code (M)edium code (H)igh code

4.2	Regularly infilled dual systems	(L) Low-rise (1-3) (M) Mid-rise (4-7) (H) High-rise (8+)	(N)o/pre code (L)ow code (M)edium code (H)igh code
4.3	Irregularly infilled dual systems (pilotis)	(L) Low-rise (1-3) (M) Mid-rise (4-7) (H) High-rise (8+)	(N)o/pre code (L)ow code (M)edium code (H)igh code

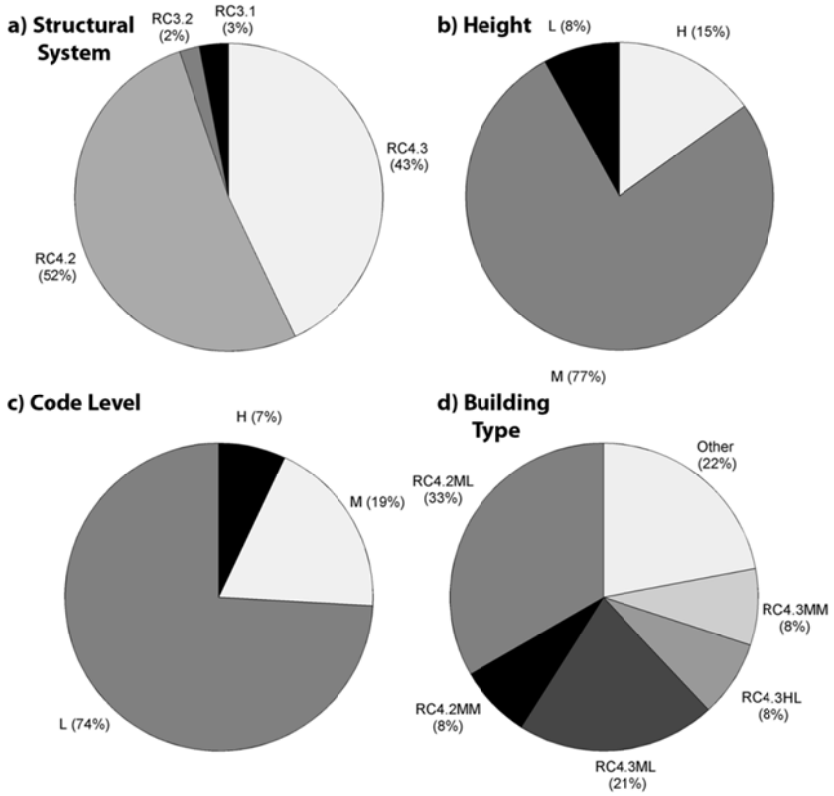

Figure 2 Classification of the RC buildings of the city of Thessaloniki based on: a) structural type, b) height, c) code level and d) building type, according to the BTM of Table 1.

3. METHODOLOGY

In this work an innovative approach is adopted to assess seismic risk in the city of Thessaloniki. The key elements of such an approach are, on one side, the use of ground motion scenarios derived from 3D physics-based numerical simulations to represent seismic hazard and, on the other side, the Capacity Spectrum Method (CSM) for the assessment of the damage of the building portfolio.

The main steps of the methodology, starting from the estimation of 3D broadband physics-based ground motions to obtain the seismic demand at each building block, up to the application of the CSM to estimate the probability of different damage states, is depicted in Figure 3. Each step is briefly described below.

Step 1. A large-scale 3D numerical model extending over considerable distances (of the order of several tens of kilometers on the horizontal scale) is constructed to simulate the seismic wave propagation phenomenon occurring during an earthquake with specified magnitude and location (scenario-based seismic hazard assessment). In this study, the historical M_W6.5 1978 Volvi earthquake has been considered. The model accounts for all factors affecting ground motion, from the features of the seismic source (represented by a kinematic model), with directivity/directionality effects due to rupture propagation along the fault, the propagation path in heterogeneous Earth media, up to the local geologic conditions within the city, which may lead to site-specific amplification patterns. The model gives as output the entire time histories of ground at any point of the model on ground surface, so that it provides a detailed picture (with resolution conditioned on mesh discretization) of variability of ground motion both in time and space. Further details on the model will be provided in Section 4.

Step 2. Ground motions computed at the previous step are limited to the low frequency range, typically up to about 1.5 Hz, as in the present case, because of the computational limitations and of our limited knowledge of the mechanical properties of the medium and of the source process at shorter wavelengths. On the other hand, damage and loss assessment studies need broadband ground motions with realistic features in a broad range of periods (say at least 0-10 Hz), covering the dominant vibration periods of all structural typologies of interest. Therefore, starting from the 3D low-frequency synthetics, broadband seismic demands are generated for each building block within the city of Thessaloniki, using the procedure illustrated in Section 4.

Step 3. For any building block, the CSM is applied: the seismic demand is compared with the capacity curve associated with the considered structural types in the spectral displacement (*SD*) – spectral acceleration (*SA*) space, to determine the performance point of the structure to this earthquake scenario. Note that the demand curve can be a design spectrum for a selected return period (e.g. Eurocode 8 design spectrum for 475 years return period), a Uniform Hazard Spectrum (UHS), computed from a PSHA study, or, as in this work, the response

spectrum of the physics-based broadband synthetics estimated at Step 2. The earthquake demand, generally provided for 5% damping, is reduced to account for the hysteretic damping associated with inelastic response of the structure, which is computed from the area enclosed by the hysteretic loop at peak response displacement and acceleration. Furthermore, a reduction factor is applied on the hysteretic damping as a function of shaking duration to account for cyclic degradation of hysteresis loops.

Step 4. The spectral displacement ($\overline{SD}$) associated with the performance point found at previous step is used as input to the fragility functions, specific for a given building typology, to determine the probability of different damage states (from no damage to collapse).

Step 5. Finally, integration of the probabilities of damage states over the different typologies allows to map the spatial distribution of damage in the city of Thessaloniki at the spatial scale of the building block.

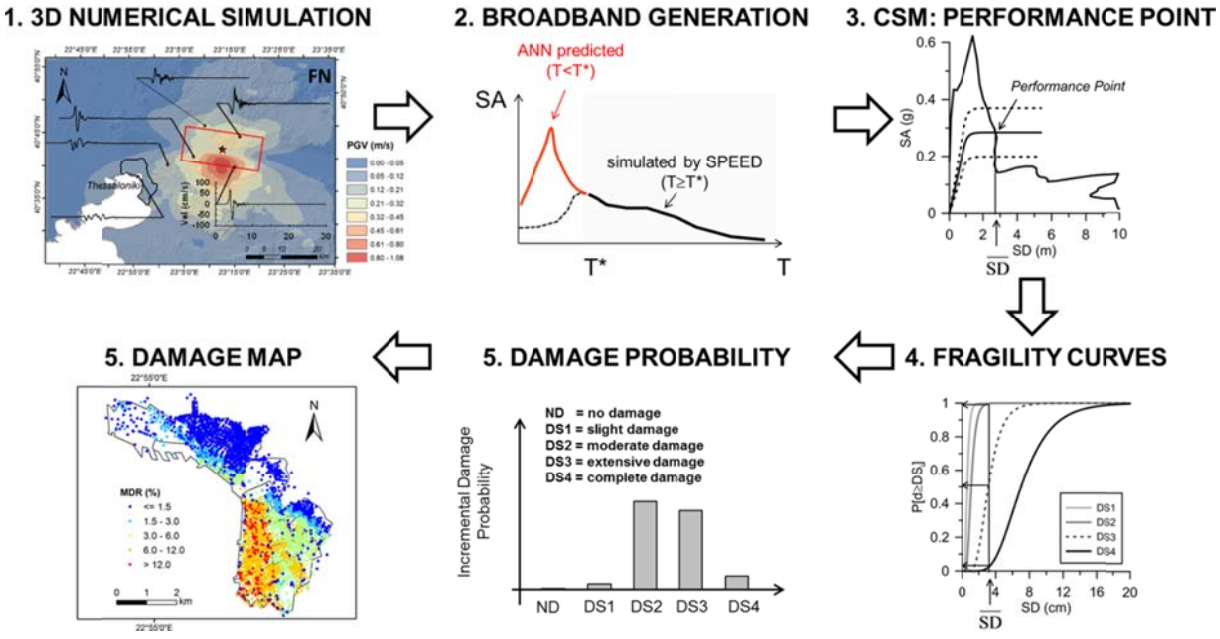

Figure 3 Methodology adopted in the present study for seismic risk assessment, with application to the city of Thessaloniki.

Referring to Steps 3 to 5, to evaluate the seismic risk in the city of Thessaloniki, the CSM implemented in the open-source software EarthQuake Risk Model - EQRM, developed by

Geoscience Australia (Robinson et al. 2005), has been adopted. Further details regarding the assumptions at the basis of the vulnerability model adopted in EQRM will be provided in Section 5.

4. 3D BROADBAND PHYSICS-BASED MODELING FOR HAZARD EVALUATION

In this study, the ground shaking in the city of Thessaloniki has been estimated through 3D physics-based numerical simulations of the M_W 6.5 June 20th 1978 Volvi earthquake. 3D modeling of earthquake ground motion in the Thessaloniki area has been addressed by the authors of this paper in a previous study (Smerzini et al. 2017), where efforts were devoted to the construction of the numerical model and the comparison of the synthetics with the observations available in terms of ground motion time histories, macroseismic intensity and site-specific amplification functions.

The numerical simulation of the Volvi earthquake was performed using the open-source computer package SPEED based on the Discontinuous Galerkin Spectral Elements Method DGSEM (http://speed.mox.polimi.it/; Mazzieri et al. 2013). Referring to Smerzini et al. (2017) for a detailed description of the numerical model, herein we limit ourselves to summarize its main features. The large-scale computational model can propagate frequencies up to about 1.5 Hz and includes, as main features, a kinematic representation of the fault rupture and a 3D subsoil model of the Thessaloniki urban area with non-linear visco elastic behavior for the shallow soil layers in the top 100 m. A sketch of the computational model adopted for the simulation of the Volvi earthquake is shown in Figure 4. To highlight the spatial variability of the ground motions predicted by numerical modeling, some representative ground motion velocity time histories (horizontal component, projected along the direction normal to the fault strike), simulated at selected observation points on ground surface, are superimposed on the numerical grid.

One of the main shortcomings of 3D physics-based numerical simulation, which strongly restricts its applicability in earthquake engineering applications, is that synthetics are reliable only in the long period range, owing to the limitations posed both by computational constraints as well as by insufficient knowledge of the medium at short wavelengths.

Increasing the maximum frequency of numerical models, from 0.2-0.5 Hz achieved in the first pioneering applications in the late 1990's, up to 2-3 Hz, has been made possible by the incessant development of computational infrastructures along with refinement of computer algorithms in a parallel environment (for a careful review see Paolucci et al. 2014). Nonetheless, such a progress is still insufficient for earthquake engineering applications, such as structural analyses and risk assessment studies, which require the use of ground motion time histories with realistic features in a broad range of vibration periods, covering the fundamental and higher vibration modes of most structures (0-10 Hz). Consider that for the portfolio of RC buildings in Thessaloniki, the fundamental elastic vibration period of the building typologies of Table 1 falls in the range 0.15-1.5 s, with most values between 0.4 s and 0.7 s.

To overcome this issue and generate broadband (referred to as BB hereinafter), ground motions usable for damage assessment purposes, we adopted a promising approach based on Artificial Neural Networks (ANN). The key points of this procedure are briefly presented herein, while for a more detailed description and verification examples we refer the reader to Paolucci et al. (2017). For any building block, the response spectral accelerations at short periods, namely at $T<T^*$, where $T^*= 0.75$ s is the minimum period of the numerical simulations, are predicted from the long period spectral ordinates ($T \geq T^*$), using an ANN previously trained on a database of recorded earthquake ground motions (namely, SIMBAD database, illustrated in Smerzini et al. 2014). Therefore, the target broadband response spectrum equals the spectrum simulated by SPEED in the long period range, while at short periods it is constructed based on the outputs of the ANN. The main advantage of this ANN-based procedure is that a correlation between the spatial variability of ground motion at long periods, simulated by the physics-based approach, and the one at short periods is naturally established.

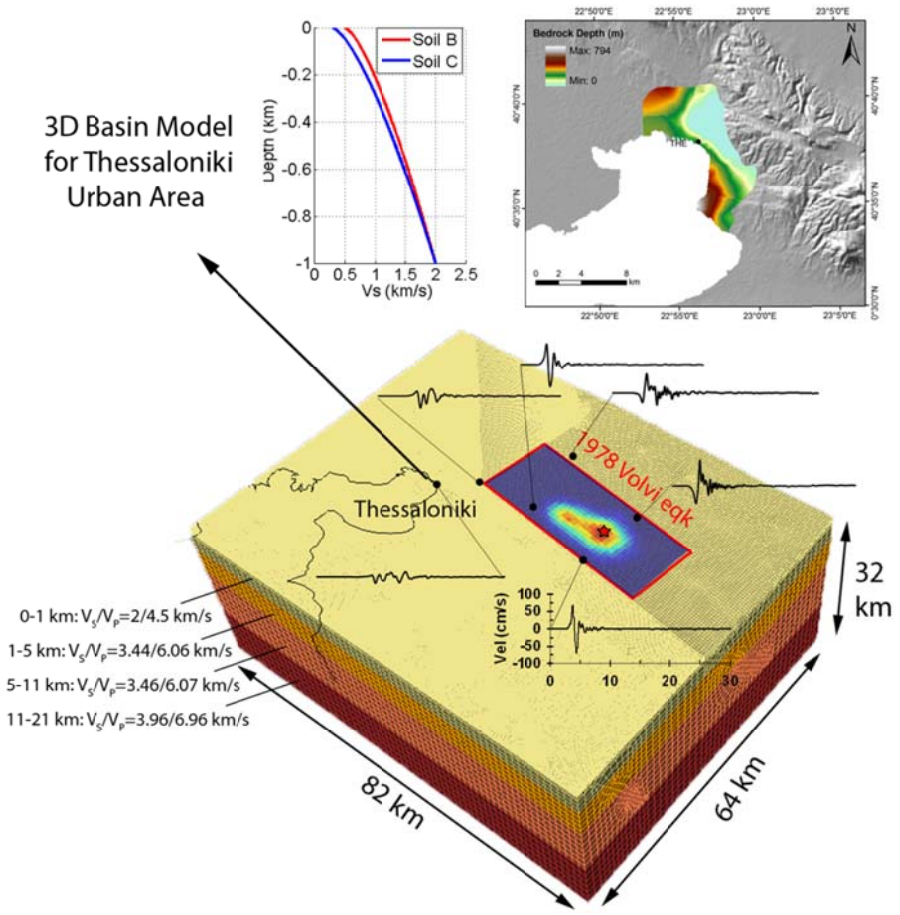

306

307 **Figure 4 Sketch of the numerical mesh adopted for the simulation of the M_W6.5 Volvi**
308 **earthquake. On the top panel the main ingredients of the 3D basin model are provided:**
309 **shear wave velocity profiles for the sediments (left) and map of bedrock depth (right).**
310 **A representative set of output velocity time histories (horizontal component normal to**
311 **fault strike) is superimposed on the model.**

312

313 Figure 5 shows the broadband response spectra *SA* (geometric mean of horizontal
314 components) obtained at selected building blocks. The results of the adopted procedure (black
315 lines) are compared with: the SPEED results (red), whose ordinates are coincident with the
316 BB ones in the long period range for T>0.75s approximately; the Uniform Hazard Spectrum
317 (UHS) from SHARE Project (Giardini et al. 2013) for 475 years return period and rock
318 conditions and then amplified according to EC8-based soil amplification factors; the 475
319 years SHARE UHS amplified according to the novel soil classification scheme proposed by
320 Pitilakis et al. (2015) (PEA15); the GMPE of Cauzzi et al. (2015) (CEA15). Referring to the
321 latter, empirical predictions were obtained considering the following parameters: M_W=6.5,

normal focal mechanism, fault distance (R_f) and V_{S30} specific for each considered site. The only available recording during the 1978 earthquake (THE station, located in the basement of an 8-storey building at the shoreline of the city) is also compared with the results for BDG 1245 (top left sub-plot of Figure 5), being the latter the closest site to the strong-motion station. Note that the synthetic response spectrum at THE station is in good agreement with the observation for almost all periods, although it tends to be higher at short periods, most likely because of the particularly low values of ground motion provided by the instrument at high frequencies, with *PGA* of around 0.15 g, associated with strong non-linear site effects and, to a minor extent, to soil-structure interaction effects. Overall, the synthetic BB spectra are in reasonable agreement with the GMPE of CEA15, although differences are found both in the short and long period range especially at soft deep sites in the southern part of the city (see e.g. BDG#1777 for T~1.5-2 s). In spite of the different nature of the *SA* from this deterministic study, which is associated with a specific earthquake scenario, and the UHS, which, instead, results from different earthquakes, being derived from a full PSHA, the comparison is still satisfactory especially when EC8-based site amplification factors are considered. The PEA15 amplified UHS represents an upper bound of the spectral ordinates for nearly all periods.

Figure 6 presents maps of *SA* computed from the 3D broadband physics-based numerical simulations (a, top panel) and from CEA15 (b, bottom panel), for selected periods, namely, *PGA*, T=0.5 s and 1 s. Empirical estimates (without any spatial correlation model) are rather homogeneous across the study area because they take into account only the attenuation with distance (which is limited for the distance ranges under consideration) and site condition (V_{S30} = 300, 500 and 800 m/s passing from the shoreline to the North-East). Empirical estimates tend to be lower than 3D simulations especially in the South-South-East part of the city owing to the directionality of fault rupture combined with long-period (T ≥ 1s) site amplification effects occurring in the deepest portion of the Thessaloniki basin. Note that such effects, reproduced by our 3D simulations, are reflected also in the short period range through the ANN-based procedure.

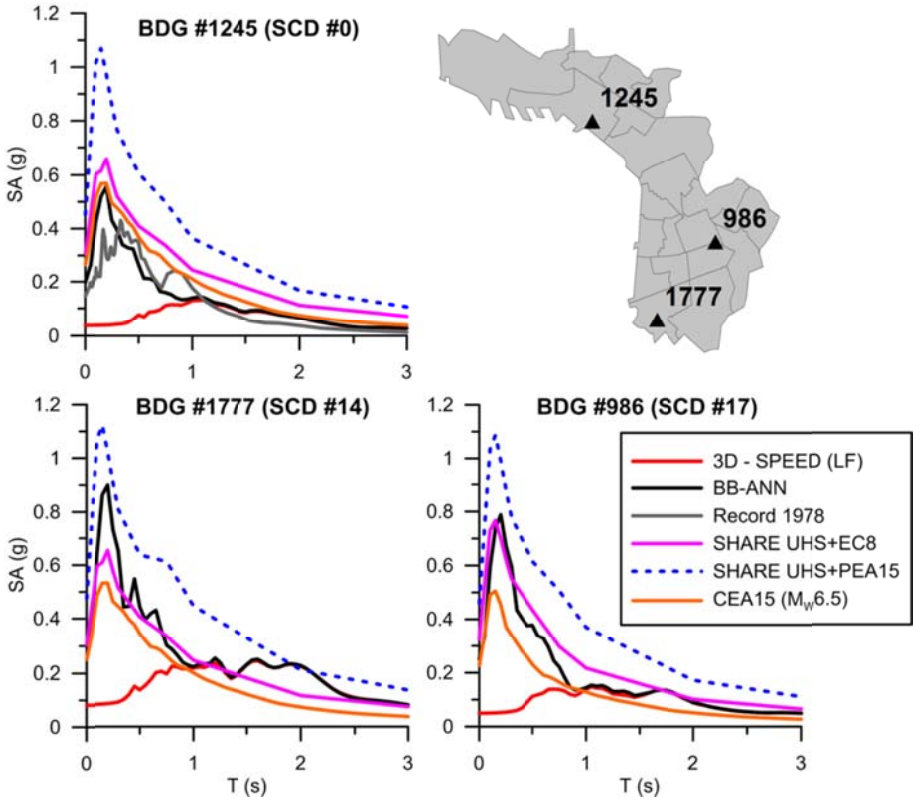

Figure 5 Broadband pseudo-acceleration response spectra (geometric mean of horizontal components, 5% damping) at selected building blocks. The 3D BB synthetics (black) are compared with: the results by SPEED (red), the 475 years return period SHARE UHS with EC8 site amplification factors (magenta), the 475 years return period SHARE UHS with the site amplification factors proposed by Pitilakis et al. (2015) - PEA15 (dashed blue), the GMPE by Cauzzi et al. (2015) - CEA145 (orange). The only available recording (grey), close to BDG #1245, is also shown in the corresponding subplot.

As mentioned in the introduction, proper modeling of spatial variability of ground motion intensity measures is relevant for risk assessment of spatially distributed portfolios in large urban areas. To assess quantitatively the spatial correlation structure of the simulated ground motion used in this work, the semivariogram γ, as a function of inter-station distance h, between residuals with respect to an average trend of $SA(T)$ has been computed using standard geostatistical tools (for further details on theoretical background the reader is referred to Jayaram and Baker 2009). Note that, in general terms, $\gamma(h)$, which is the complement of the correlation coefficient, provides a measure of the average dissimilarity of the response spectral accelerations obtained at a separation distance h. The results are illustrated in Figure

7, where the semivariogram values $\gamma(h)$ associated with *SA(0.5s)*, on the left, and *SA(1.0s)*, on the right, for a large suite of receivers falling in the urban area and in the surroundings are plotted. Note that, for this geostatistical analysis, it was necessary to consider a set of receivers sampling a wider area than the one adopted for risk computations to adequately catch the overall trend of $\gamma(h)$ over a suitable range of inter-station distances. In Figure 7 the least-squares best-fitting exponential model (dashed lines), which is the commonly adopted model in literature, is also shown. It turns out that the spatial correlation of response spectral ordinates of ground motion is realistically reproduced both at short and long periods, with an average behavior of semivariogram across multiple sites for increasing inter-station distances and for different structural periods in agreement with studies based on recorded ground motions (see e.g. Jayaram and Baker 2009; Esposito and Iervolino 2012). On the other hand, the use of GMPEs would produce a semivariogram equal to zero at all inter-station distances. Specifically, the range of semivariograms, i.e. the inter-station distance at which the semivariogram γ tends to a plateau or, in other words, the correlation drops to zero (see superimposed arrows in Figure 7) turns out to be equal to around 39 km and 49 km for *SA(0.5s)* and *SA(1.0s)*, respectively, with a tendency to increase for longer periods, in agreement with the research works previously cited. It is noted that the rather high values of ranges obtained here are consistent with the values found by Jayaram and Baker (2009) for selected earthquakes (e.g. the 1999 Chi-Chi earthquake in Taiwan; the 2003 Big Bear City earthquake in USA) and may be attributed to the clustering of V_{S30} values, as for the case of Thessaloniki.

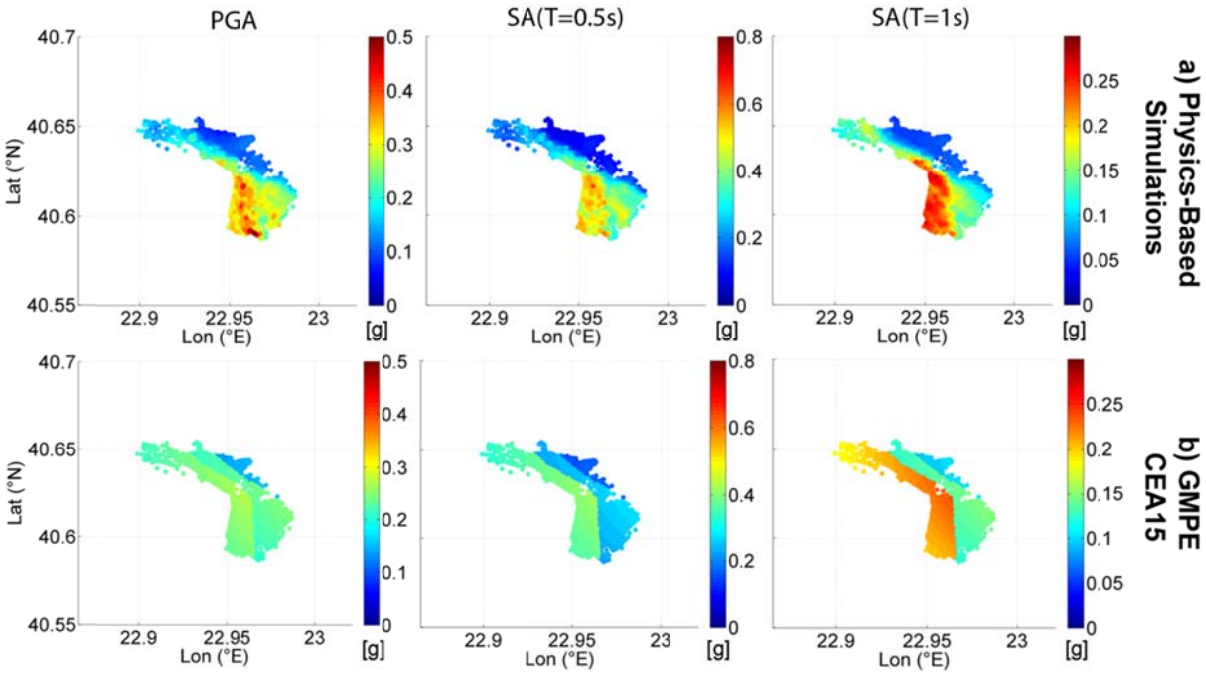

391

392 **Figure 6 Spectral acceleration maps (in g, 5% damping), geometric mean of horizontal**
393 **components, for selected periods, (*PGA*, *T*=0.5 and 1 s), from BB physics-based**
394 **simulations (a, top) and from the GMPE of CEA15 (b, bottom). Note that a different**
395 **scale of the colorbar is adopted for graphical purposes.**

396

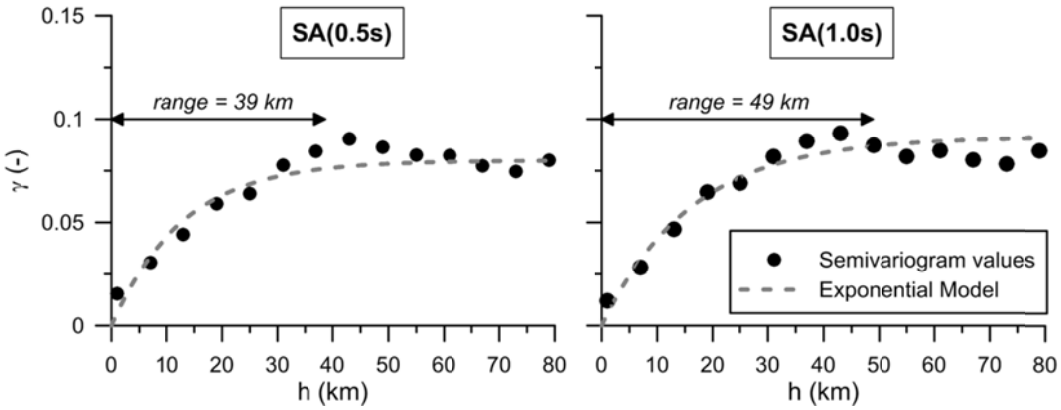

397

398 **Figure 7 Evaluation of spatial correlation of 3D broadband physics-based ground motions in**
399 **terms of semivariogram γ, as a function of inter-station distance *h*, for *SA(0.5s)*, left,**
400 **and *SA(1.0s)*, right. The least-squares best-fitting exponential models are shown by the**
401 **dashed lined and the corresponding ranges are indicated by the superimposed arrows.**

402

403

404

5. VULNERABILTY MODEL

As described in Section 3, the CSM has been adopted to estimate the expected damage of the RC building stock in the Thessaloniki urban area when subjected to the 1978 earthquake-like scenario. The CSM requires the definition of the capacity and displacement-based fragility curves for each building typology. In this study, the capacity and fragility curves developed by the Aristotle University of Thessaloniki - AUTH (Kappos et al. 2006; D'Ayala et al. 2012) are used. In the following further details regarding both capacity and fragility curves will be provided.

The capacity curves were first obtained by Kappos et al. (2006) specifically for the Greek buildings in Thessaloniki area using a hybrid approach, where statistical data from earthquake-damaged buildings were combined with results of non-linear dynamic or static analyses. For all Low and High code RC (see Table 1) buildings capacity curves were derived on the basis of a pushover analysis using 2D models, where RC members were modeled using lumped plasticity beam-column elements, while infill walls were modeled using the diagonal strut element. Under the hypothesis of a 2D model, the effects of plan irregularity and, thus, torsional effects, were neglected; however, as discussed in Kappos et al. (2006), such effects are found to have a minor impact on the overall loss estimates in the city of Thessaloniki and are less influential than irregularities in elevation (e.g. presence of soft storeys), which were explicitly accounted for. Based on these numerical analyses empirical corrections were then applied to produce curves for the pre-code and moderate-code buildings.

The capacity curves for the most frequent building typologies, RC4.2ML, RC4.3ML, RC4.2MM, RC4.3HL and RC4.3MM, are presented in Figure 8 in the standard bilinear form, defined by the yield point (SD_y, SA_y) and ultimate point (SD_u, SA_u). However, it should be underlined that in the EQRM code the capacity curve is modelled in such a way (specifically, the non-linear part from the yield point to the ultimate point is modeled as an exponential function) that strain-hardening is scarcely accounted for and this may play a role especially for concrete walls buildings. The uncertainty associated with the capacity curve is taken into account in the computations by describing the ultimate spectral acceleration SA_u as a aleatory variable following a log-normal probability distribution with standard deviation $\beta_u = 0.3$, as recommended in FEMA (1999).

Fragility curves define the probability that the expected damage d of a particular building or building class exceeds a given damage state DS_i, as a function of a parameter quantifying the severity of the seismic demand, which is, in the CSM, the spectral displacement SD. In the code EQRM, fragility curves are provided for four different damage states, namely, slight, moderate, extensive and complete, and for both structural and non-structural damage. In the present study only structural damage has been considered. The fragility functions are assumed to follow a log-normal distribution such that the conditional probability of exceeding a certain damage state DS_i is given by the following expression:

$$P[\, d \geq DS_i \,] = \Phi\left[\frac{ln\left(SD / S_{T,DS_i}\right)}{\beta_{SDi}}\right] \quad (1)$$

where $\Phi(\cdot)$ is the standard normal cumulative distribution function, S_{T,DS_i} is the median value of spectral displacement corresponding to the spectral displacement threshold associated with the damage state DS_i and β_{DS_i} is the logarithmic standard deviation. Therefore, under this assumption, for each building typology, the fragility curve is completely defined by only two parameters: the mean spectral displacement S_{T,DS_i} and the corresponding standard deviation β_{DS_i}.

The displacement thresholds for the Greek RC buildings were defined by D'Ayala et al. (2012) as a function of the yield and ultimate spectral displacement, for five damage states, namely, DS1 (slight), DS2 (moderate), DS3 (substantial to heavy), DS4 (very heavy) and DS5 (collapse), as described in Table 2. As in EQRM only four damage states are defined, following other studies (see Pitilakis et al. 2015; Riga et al. 2017), the damage states have been modified as follows: DS1 for slight damage, DS2 for moderate, DS3 for extensive, while DS4 and DS5 damage states have been combined to express complete damage state (DS5 is taken for complete damage). For the logarithmic standard deviation of fragility, a value β_{DS_i} = 0.4, for all damage states, was assumed based on the recommendations in FEMA (1999). The resulting fragility curves are illustrated in Figure 9 for the same building typologies as presented in Figure 8.

In the computations, reduction of spectral values to account for the hysteretic damping associated with the inelastic behavior of structures is carried out using the reduction factors proposed by HAZUS methodology and considering a moderate duration corresponding to earthquakes of magnitude in the range between 5.5 and 7.5.

It is worth underlining that analysis of the effect of assumptions in the vulnerability model, such as absence of strain-hardening effects in the capacity curve and merging of damage states DS4 and DS5, which were essentially dictated by the restraints of the EQRM code, has not been addressed herein as the primary goal of this work was to demonstrate the feasibility of incorporating 3D physics-based scenarios into seismic risk assessment studies at urban scale.

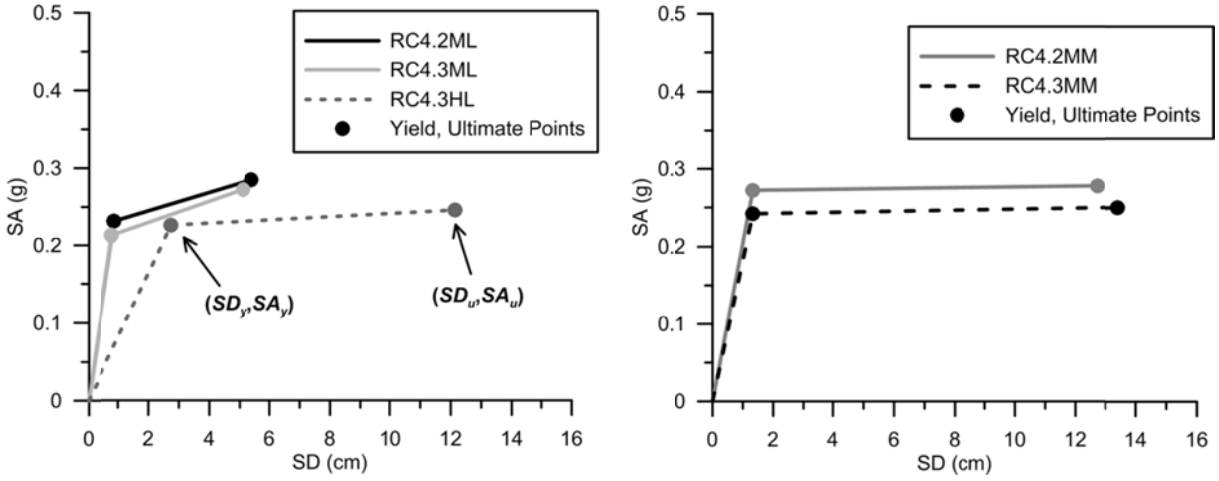

Figure 8 Capacity curves for the most frequent building types in the city of Thessaloniki according to Kappos et al. (2006) and D'Ayala et al. (2012). Left: low-code buildings (RC4.2ML, RC4.3ML and RC4.3HL), right: medium-code buildings (RC4.2MM and RC4.3MM).

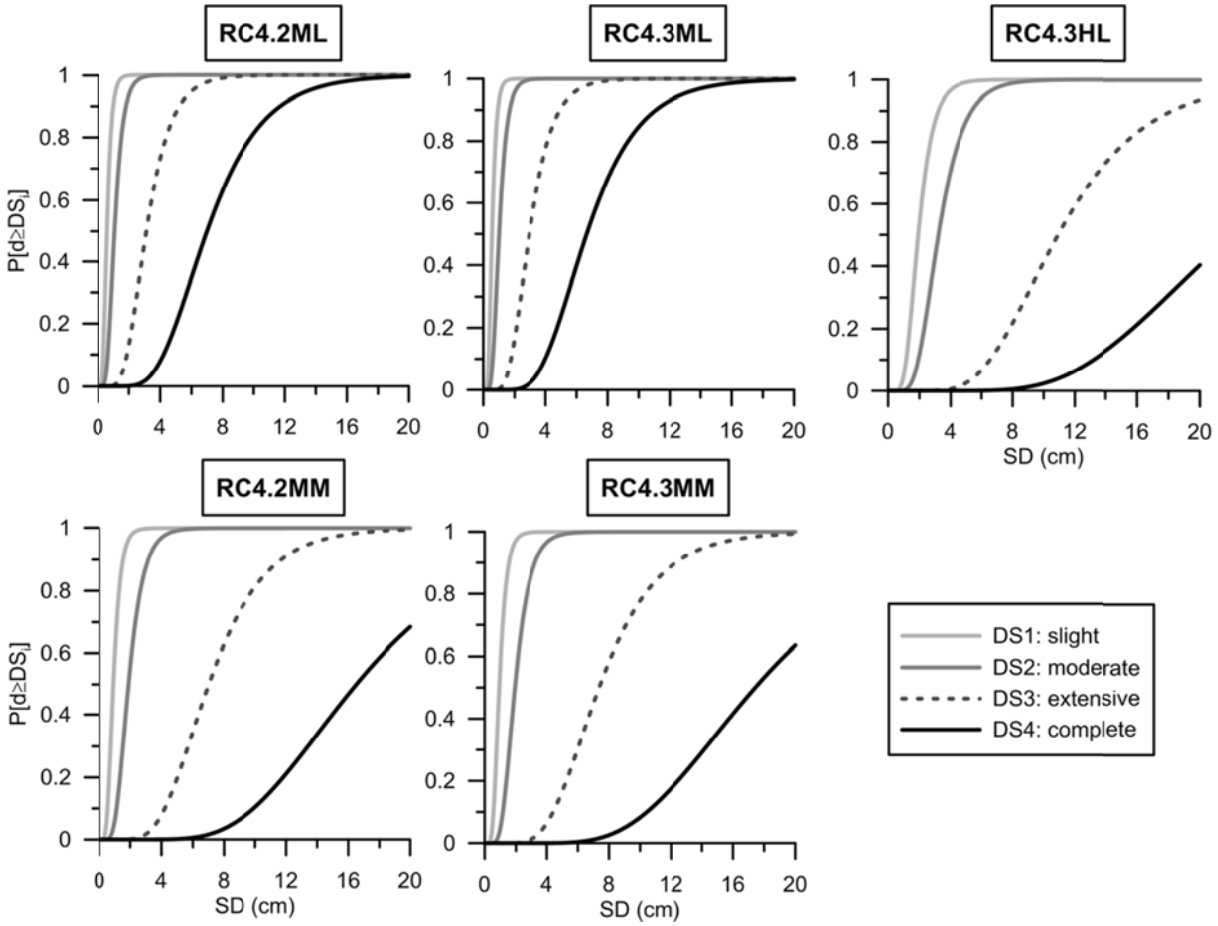

Figure 9 Fragility curves for the most frequent building types in the city of Thessaloniki based on D'Ayala et al. (2012): RC4.2ML, RC4.3ML, RC4.2MM, RC4.3HL and RC4.3MM.

Table 2 Damage state displacement thresholds, from D'Ayala et al. (2012). SD_y and SD_u denote the yield and ultimate displacement, respectively.

Damage State	Bare frames		Bare dual	
	Infilled frames $SD_{u,bare} < 1.1\ SD_u$	Infilled frames $SD_{u,bare} \geq 1.1\ SD_u$	Infilled dual-shear wall drop strength	Infilled dual-infill walls failure
DS1 (slight)	$0.7 \cdot SD_y$		$0.7 \cdot SD_y$	
DS2 (moderate)	$SD_y + 0.05 \cdot (SD_u - SD_y)$		$SD_y + 0.05 \cdot (SD_u - SD_y)$	
DS3 (substantial to heavy)	$SD_y + 1/3 \cdot (SD_u - SD_y)$	$SD_y + 1/2 \cdot (SD_u - SD_y)$	$SD_y + 1/2 \cdot (SD_u - SD_y)$	$0.9 \cdot SD_u$
DS4 (very heavy)	$SD_y + 2/3 \cdot (SD_u - SD_y)$	SD_u	SD_u	$SD_{u,bare}$
DS5 (collapse)	SD_u	$SD_{u,bare}$	$1.3 \cdot SD_u$	$1.3 \cdot SD_{u,bare}$

6. RESULTS: DAMAGE AND LOSS SCENARIO

Coupling of the broadband physics-based ground shaking scenario with the vulnerability model of the RC building block allows to estimate the spatial distribution of the expected damage in the urban area of Thessaloniki during the historical 1978 earthquake. Results of the seismic risk scenario in terms of structural damage are presented in this Section and then compared with the post 1978 earthquake damage observations.

Figure 10 presents the spatial distribution of the percentage of building floor area (FA) in the four damage states, from slight to complete (collapse), within in the city of Thessaloniki, building block by building block. For each building block and each damage state, the damaged FA is computed by multiplying the probabilities of exceeding the damage state for any building typology by the FA associated with all buildings of the given type and within the considered building block and, then, by integrating these quantities over all building typologies. For graphical purposes, data for each DS are grouped using the natural break classification implemented in ArcGIS software. Although the damage is computed building block by building block, it is useful to show the damaged FA also at the aggregated level of the sub-city districts (SCD), as illustrated in Figure 11. In this figure, in addition to the damaged FA (right), the Mean Damage Ratio (MDR) per SCDs is also reported. The MDR represents the total cost of repair normalized with respect to the reconstruction cost and is computed using the following relationship:

$$MDR = \sum_{i=1}^{4} FA_{DS_i} \cdot LI_i \qquad (2)$$

where FA_{DS_i} is the percentage of FA in damage state i and LI_i denotes the corresponding loss index for RC structures, according to Kappos et al. (2008), see Table 3.

Overall, it turns out that about 23% of the RC buildings undergoes slight damage, 38% moderate damage, 8% extensive damage and 0.3% complete damage. Higher damages are found predominantly in the South-South-East sector of the urban area, where higher seismic demands are found especially in the range of periods T=0.4-0.7 s, corresponding to the fundamental vibration period of the most common building types. Intermediate to long period amplification of ground motion in the southern sector of the city is mainly associated with

local site amplification combined with effects coming from the extended source; by application of the ANN procedure, such effects are also reflected on the short period spectral ordinates. To better understand this, it is underlined that the 3D geological model includes homogeneous velocity profiles, with lowest values of shear wave velocity close to the shoreline, and the depth of geologic bedrock reaches the maximum depth, of the order of 700-800 m, in the southern part of the city (see Figure 4, top panel).

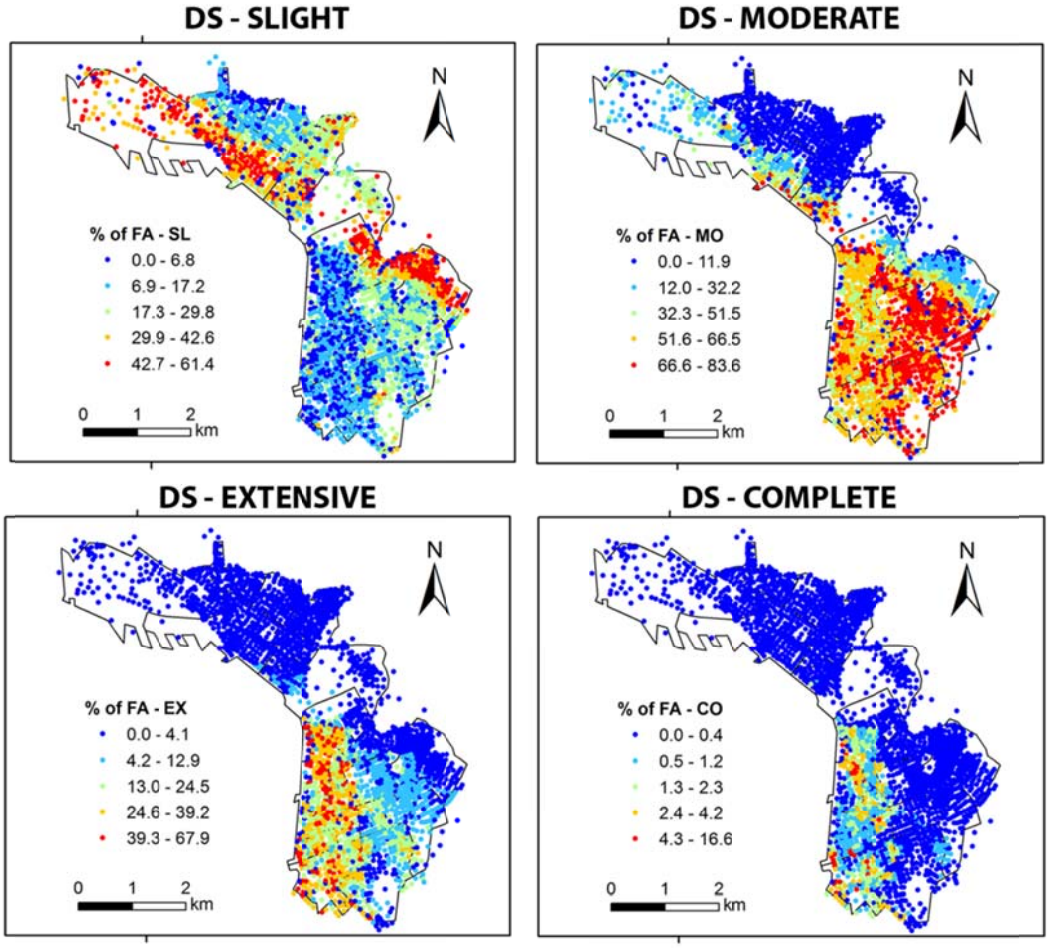

Figure 10 Spatial distribution of damage in the city of Thessaloniki for the M_W6.5 1978 earthquake in terms of percentage of floor area (FA) in the four damage states, slight, moderate, extensive and complete.

A quantitative comparison with the damage scenario obtained using a standard empirical approach for ground motion prediction is shown in Figure 12. Specifically, in this figure we

report the spatial distribution of the MDR (per building block) obtained from: a) 3D physics-based numerical simulations and b) the GMPE of CEA15 (see also Figure 7), for the same target scenario corresponding to the M_W6.5 1978 earthquake. Note that no spatial correlation model has been applied to empirical estimates to consider the approach that is routinely adopted in engineering practice. Overall, with respect to the 3D-based scenario, the extent of extensive and complete damage provided by CEA15 turns out to be lower, especially in the southern sector of the city. For CEA15, the total percentages of slight, moderate, extensive and complete damage are 34.7%, 48%, 3% and 0.02%, respectively. Therefore, in spite of a general agreement of 3D-based simulations with empirical models in terms of average estimates, as demonstrated in Smerzini et al. (2017), differences in the spatial variability of ground motion intensities in the urban area of Thessaloniki may have a strong impact on damage assessment.

Table 3 Loss indices for RC buildings according to Kappos et al. (2008).

Damage State	Central Loss Index (%)
DS1-slight	0.5
DS2-moderate	5
DS3-extensive	20
DS4-complete	80

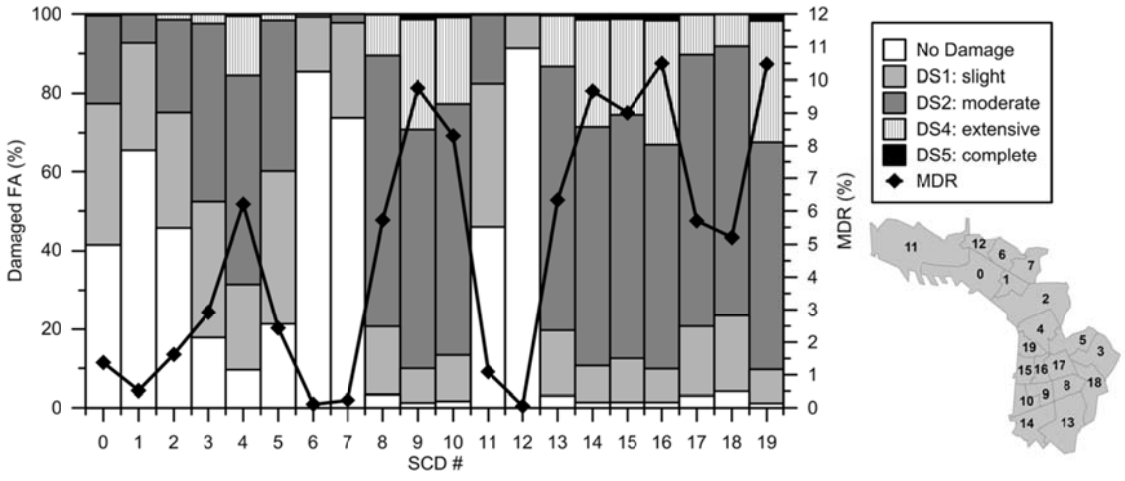

Figure 11 Damage distribution per sub-city districts (SCDs) in terms of: left, % of damaged FA and, right, Mean Damage Ratio (MDR, in %). The location of the SCDs is shown on the bottom right map.

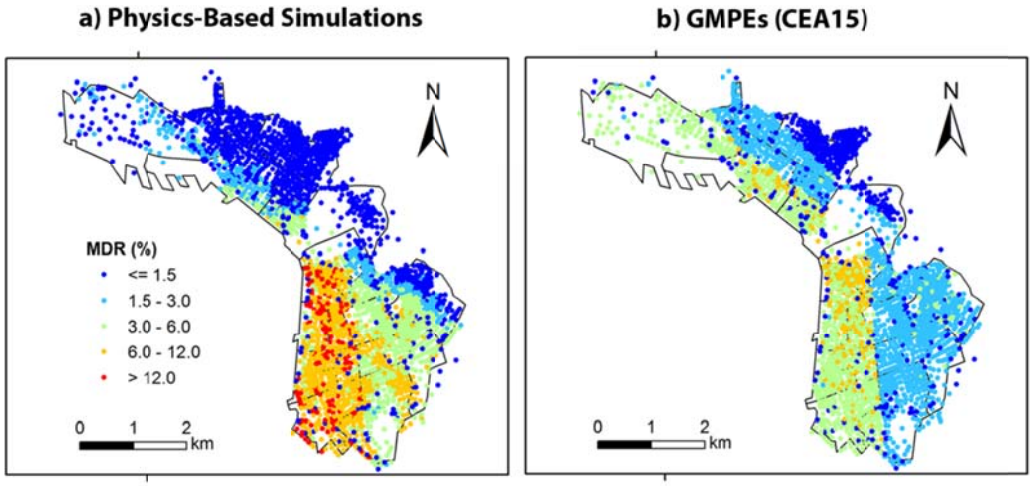

Figure 12 Comparison of damage scenarios (MDR, in %) obtained from: a) 3D physics-based numerical simulations and b) the GMPEs of CEA15 for the same target ground motion scenario (M_W6.5 1978 earthquake).

One of the most critical issues in the development of seismic risk assessment tools, especially when applied to large urban areas, is the validation against real earthquakes, which is only rarely addressed. In the following, to verify the reliability of the damage estimates obtained through the proposed approach, a comparison with the actual post 1978 earthquake damage observations will be presented and discussed. However, when comparing our results with the available observations, it should be considered that the building stock considered in these analyses do not reflect exactly the situation at the time of the earthquake in terms of density of the buildings, typology (masonry structures which suffered serious damage during the earthquake are not considered herein) and code design level (in 1978 all buildings were designed and constructed according to the 1959 code or no code at all).

Following the 20 June 1978 mainshock with its devastating socio-economic impact, a number of studies were carried out to investigate the damage distribution within the city of Thessaloniki, based on the use of questionnaires, as traditionally applied in Greece (Leventakis, 2003), on the statistical treatment of loss data (Penelis et al. 1988; Kappos et al. 1991) and on the combined analysis of questionnaire and expert judgement datasets (Panou et al. 2014). Leventakis (2003) estimated the spatial distribution of the macroseismic intensity according to the modified Mercalli scale MSK with an accuracy of ± 0.1, by processing the questionnaires distributed to the Thessalonki citizens (see Figure 13b). In parallel to this

565 work, Kappos et al. (1991) mapped the post 1978 earthquake losses in terms of cost of repair
566 per unit area for a part of the city, i.e. the central (*intramuros*) part and a major South-East
567 sector (see Figure 13c). More recently, Panou et al. (2014) merged the damage datasets
568 coming from the traditional questionnaire-based study and from in-situ inspections by expert
569 engineers to compile a map in terms of European Macroseismic scale EMS-98.

570 Figure 13 presents a qualitative comparison of the results of our study in terms of spatial
571 distribution of MDR (a) with the MSK map compiled by Leventakis (2003) (b) as well as the
572 repair costs estimated by Kappos et al. (1991) (c). Considering the assumptions in our
573 analyses and differences between the actual and modelled building stock, the comparison can
574 be considered reasonable, especially with Kappos et al. (1991). With respect to Leventakis
575 (2003), less conservative damage estimates are found in the north-western and central
576 (*intramuros*) sector of the city; referring to the latter, where serious damages have been
577 reported, underprediction may be due to the peculiar soil conditions (i.e., presence of 5-15 m
578 thick debris of the ancient Hellenistic and Byzantine city), which could not be taken into
579 account in the 3D model with a sufficient level of resolution, and to the fact the our risk
580 analyses do not include the masonry buildings.

581 As a further comparison, we considered the damage statistics provided by Penelis (2008),
582 where the damaged buildings are classified according to the familiar “Green”, “Yellow” and
583 “Red” tag scheme. Consider that this study covers the same portion of the city (central -
584 *intramuros* part and a major S-SE sector) as considered in Kappos et al. (1991). The
585 correspondence between tag color and DS adopted in our damage computations was assumed
586 as follows: “Green” = DS0 (no damage) + DS1 (slight) + 30%·DS2 (moderate); “Yellow” =
587 70%·DS2 (moderate) + 50%·DS3 (extensive); “Red” = 50% DS3 (extensive) + DS4
588 (complete). The 30%-70% partition of DS2 between “green” and “yellow” was based on the
589 previous study by Pitilakis et al. (2015), while for the “red” tag it was decided to include a
590 good proportion of buildings in DS3 (extensive) since in our computations DS4 corresponds
591 only to collapse. This choice is in line with the considerations provided by Kappos et al.
592 (2008). The comparison of our damage predictions with the statistics provided by Penelis
593 (2008) is reported in Table 4 together with the results obtained with two robust GMPEs for
594 shallow crustal earthquakes, namely CEA15 (already considered in previous comparisons)
595 and Akkar et al. (2014), referred to as AEA14. It turns out that overall the results of this study

are in satisfactory agreement with the observations and reproduces noticeably well the percentage of seriously damaged buildings ("red" buildings). On the other hand, the two GMPEs are substantially consistent with one another but provide strongly unsafe estimates of the most affected class of buildings, of a factor of about 3. Also for "green" and "yellow" classes 3D physics-based simulation provides a slightly better fit with actual damage statistics than the GMPEs, although, in general, all methods provide comparable results with a tendency of being more conservative. For this specific case study, the relatively good performance of empirical ergodic approaches is related to the very detailed knowledge of the parameters involved in the prediction (i.e. soil mapping in terms of V_{S30} derived from microzonation studies), which is hardly available for other cities.

Table 4 Comparison of the damage statistics provided by in Penelis (2008) with this study and the GMPEs of CEA15 and AEA14, according to the tag scheme "Green", "Yellow" and "Red" (see text for further details).

Building Tag	Observed (%)	This study (%)	CEA15 (%)	AEA14 (%)
Green	74.5	65.0	63.3	60.9
Yellow	21.0	30.6	35.1	37.4
Red	4.5	4.3	1.5	1.7

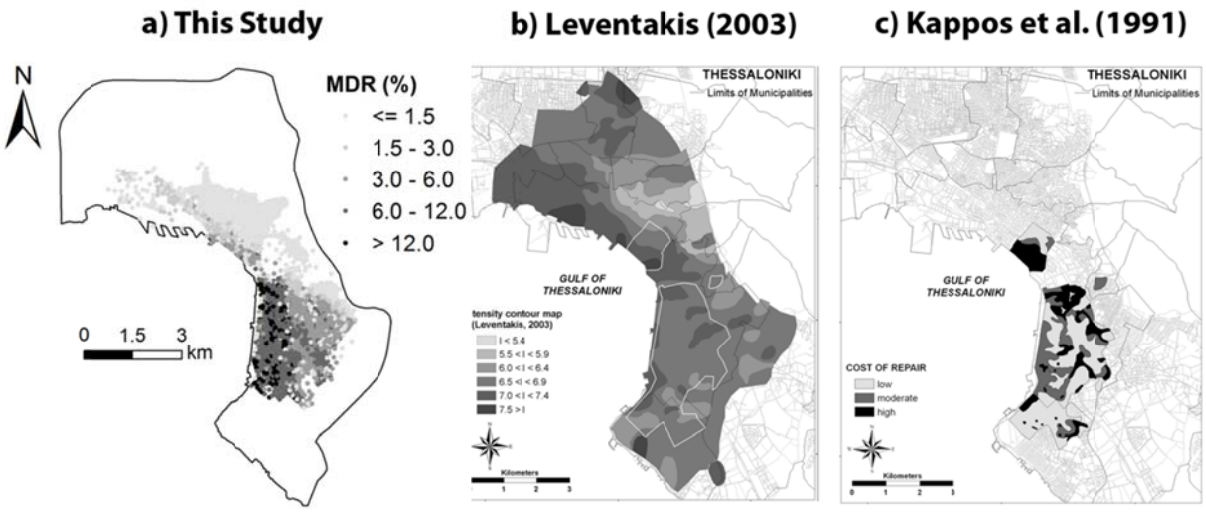

Figure 13 Comparison of damage prediction obtained from: a) this study based on 3D physics-based numerical simulations in terms of MDR (%); b) macroseismic MKS intensity observations elaborated by Leventakis (2003); c) distribution of repair cost according to Kappos et al. (1991). The maps in b) and c) are taken from Panou et al. (2014).

7. CONCLUSIONS

In this study we have shown an innovative approach for seismic risk assessment in large urban areas relying on next-generation tools for the prediction of earthquake ground shaking, based on 3D broadband physics-based numerical simulations including the seismic fault rupture, the complete propagation path from the source to the site and local complex site conditions (topographic and basin-edge effects). Referring to the vulnerability model, displacement-based fragility functions are adopted in a performance-based assessment framework like the Capacity Spectrum Method. The use of fragility functions defined in terms of response spectral displacement, as compared to more traditional fragility functions compiled as function of short period intensity measures (e.g. *PGA*), allows us to fully exploit the capabilities of 3D approaches, which are known to perform better in the long period range owing to computational limits.

To verify the feasibility and advantages of using 3D physics-based simulations for risk assessment studies, the physical damage scenario for the RC building stock of the urban area of Thessaloniki during the M_W6.5 June 20th 1978 earthquake has been estimated and compared with the damage observations. Significant damages are found predominantly along the shoreline, especially in the central-southern sector of the city, where high spectral accelerations are obtained in the short to intermediate range of periods (0.4-0.7 s), corresponding to the fundamental vibration mode of the most common building types. In these zones of the city ground motions are amplified primarily owing to local site conditions and, secondarily, to directionality effects coming from the extended source. It has been proved that a satisfactory comparison with the post 1978 earthquake damage observations can be achieved using 3D physics-based numerical modeling, especially in reproducing the extent of heavily damaged buildings, and that such a fit cannot be achieved by standard empirical approaches.

This study demonstrates the advantages of using a non-ergodic approach for ground motion prediction based on 3D physics-based numerical simulations, rather than standard empirical approaches, in seismic risk assessments, in relation to different aspects, namely, (i) the capability to reproduce realistically the spatial correlation structure of ground motions, which is of paramount importance for damage evaluations in large urban environments; (ii) the

detailed prediction of ground shaking in the near-source region of large earthquakes and in complex geologic conditions with peculiar amplification patterns; (iii) the reliable assessment of damage distribution, as compared with observations during real earthquakes.

Although the seismic risk estimates presented in this work are limited to a single case study and a single scenario within a deterministic framework, extension to further case studies can be easily accomplished, provided that a detailed knowledge regarding both the geologic context as well as the portfolio of assets is available to calibrate with sufficient accuracy a 3D model. Nowadays, 3D physics-based numerical modeling has become mature enough to be incorporated also into a probabilistic framework (see e.g. Graves et al. 2011; Villani et al. 2014; Stupazzini et al. 2017) and future research will certainly move towards its integration into advanced probabilistic seismic risk assessment tools.

ACKNOWLEDGEMENTS

This study has been carried out in the framework of the STREST Project "Harmonised approach to stress tests for critical infrastructures against natural hazards", EU FP7/2007-2013, grant agreement no. 603389. The authors are grateful to Evi Riga and Anna Karatzetzou for relevant discussion on the EQRM analyses and to Areti Panou for sharing the maps on the damage observations during the 1978 earthquake. The authors extend their gratitude to Kiana Hashemi for her contributions in early stages of this work, to Filippo Gatti for his support to generate the broadband ground motions, to Maria Infantino for helping in computing the semi-variograms of simulated motions, to Marco Stupazzini and Roberto Paolucci for their fruitful remarks. The remarks of an anonymous reviewer are also acknowledged.

669 **REFERENCES**

670 Akkar S, Sandikkaya MA, Bommer JJ (2014) Empirical ground-motion models for point- and
671 extended-source crustal earthquake scenarios in Europe and the Middle East, *Bull*
672 *Earthq Eng* 12(1): 359-387.
673 Anastasiadis A, Raptakis D, Pitilakis K (2001) Thessaloniki's detailed microzoning:
674 subsurface structure as basis for site response analysis. *Pure Appl Geophys* 158(12):
675 2597-2633
676 Apostolidis P, Raptakis D , Roumelioti Z, Pitilakis K (2004) Determination of S-wave
677 velocity structure using microtremors and SPAC method applied in Thessaloniki
678 (Greece). *Soil Dyn Earthq Eng* 24: 49-67
679 Argyroudis S, Selva J, Kakderi K, Pitilakis K (2014) Application to the city of Thessaloniki,
680 in *SYNER-G: Systemic Seismic Vulnerability and Risk Assessment of Complex Urban,*
681 *Utility, Lifeline Systems and Critical Facilities*, Vol. 31 of the series Geotechnical,
682 Geological and Earthquake Engineering, Chap 7, pp 199-240
683 ATC (1996) Seismic Evaluation and Retrofit of Concrete Buildings. Report ATC-40, Applied
684 Technology Council, Redwood City, California, U.S.A.
685 Barbat AH, Pujades LG, Lantada N. (2008) Seismic damage evaluation in urban areas using
686 the capacity spectrum method: Application to Barcelona. *Soil Dyn Earthq Eng*
687 28:851–65. http://dx.doi.org/10.1016/j.soildyn.2009.12.014.
688 Bielak J, Graves RW, Olsen KB, Taborda R, Ramirez-Guzman L, Day SM, Ely GP, Roten D,
689 Jordan TH, Maechling PJ, Urbanic J, Cui Y, Juve G (2010) The ShakeOut earthquake
690 scenario: Verification of three simulation sets. *Geophys J Int* 180: 375–404.
691 Calvi GM, Magenes G, Bommer JJ, Pinho R, Crowley H, Restrepo-Vélez LF. (2006)
692 Displacement-based methods for seismic vulnerability assessment at variable
693 geographical scales. *ISET J Earthq Technol*, 43(3): 75–104
694 Cauzzi C, Faccioli E, Vanini M, Bianchini A (2015) Updated predictive equations for
695 broadband (0.01–10s) horizontal response spectra and peak ground motions, based on
696 a global dataset of digital acceleration records. *Bull Earthq Eng* 13(6):1587–1612. doi:
697 10.1007/s10518-_ 014-_9685-_y.

CEN, European Committee for Standardization (2004) Eurocode 8: Design Provisions for Earthquake Resistance of Structures, Part 1.1: General Rules, Seismic Actions and Rules for Buildings.

Chaljub E, Moczo P, Tsuno S, Bard PY, Kristek J, Kaser M, Stupazzini M, Kristekova M (2010) Quantitative comparison of four numerical predictions of 3D ground motion in the Grenoble Valley, France. *Bull Seismol Soc Am* 100 (4): 1427–1455

D'Ayala D, Kappos A, Crowley H, Antoniadis P, Colombi M, Kishali E, *et al.* (2012) Providing building vulnerability data and analytical fragility functions for PAGER. Final Technical Report. Oakland, California, USA.

Erdik M, Aydinoglu N, Fahjan Y, Sesetyan K, Demircioglu M, Siyahi B, Durukal E, Ozbey C, Biro Y, Akman H, Yuzugullu O (2003) Earthquake risk assessment for Istanbul metropolitan area. *Earthq Eng and Eng Vibr* 2(1): 1-23. doi:10.1007/BF02857534.

Esposito S, Iervolino I (2011) PGA and PGV spatial correlation models based on European multievent datasets. *Bull Seismol Soc Am* 101(5): 2532–2541

Esposito S, Iervolino I (2012) Spatial correlation of spectral acceleration in European data. *Bull Seismol Soc Am* 102(6): 2781–2788

FEMA (1999). HAZUS99 Technical Manual. Federal Emergency Management Agency, Washington, DC, U.S.A.

Freeman SA (2004) Review of the development of the capacity spectrum method. ISET J Earthq Technol 41:1–13.

Gallovič F (2016) Modeling velocity recordings of the Mw6.0 South Napa, California, earthquake: unilateral event with weak high-frequency directivity. *Seismol Res Lett* 87: 2-14.

Giardini D, Woessner J, Danciu L, Crowley H, Cotton F, Grünthal G, Pinho R, Valensise G, Akkar S, Arvidsson E, Basili R, Cameelbeeck T, Campos-Costa A, Douglas J, Demircioglu MB, Erdik M, Fonseca J, Glavatovic B, Lindholm C, Makropoulos K, Meletti C, Musson R, Pitilakis K, Sesetyan K, Stromeyer D, Stucchi M, Rovida A (2013) Seismic Hazard Harmonization in Europe (SHARE): Online Data Resource, doi: 10.12686/SED-00000001-SHARE.

Graves G, Jordan TH, Callaghan S, Deelman E, Field E, Juve G, Kesselman C, Maechling P, Mehta G, Milner K, Okaya D, Small P, Vahi K (2011) CyberShake: a physics-based

729 seismic hazard model for Southern California, *Pure appl. Geophys.*, 168(3–4): 367–
730 381.
731 Jayaram N, Baker JW (2009) Correlation model of spatially distributed ground motion
732 intensities. *Earthq Eng Struct Dyn* 38:1687–1708
733 Jayaram N, Baker JW (2010) Efficient sampling and data reduction techniques for
734 probabilistic seismic lifeline risk assessment. *Earthq Eng Struct Dyn* 39(10):1109–
735 1131
736 Kappos A, Stylianidis K, Penelis G (1991) Analytical prediction of the response of structures
737 to future earthquakes. *Eur Earthq Eng* 1:10–21
738 Kappos AJ, Panagopoulos G, Panagiotopoulos C, Penelis G (2006) A hybrid method for the
739 vulnerability assessment of R/C and URM buildings. *Bull Earthq Eng* 4(4):391–413.
740 http://dx.doi.org/10.1007/s10518-006-9023-0.
741 Kappos AJ, Panagopoulos GC, Penelis GG (2008) Development of a seismic damage and loss
742 scenario for contemporary and historical buildings in Thessaloniki, Greece. *Soil Dyn*
743 *Earthq Eng* 28(10–11), 836–850
744 Leventakis GA (2003) Microzonation study of the city of Thessaloniki. PhD Thesis, Aristotle
745 University of Thessaloniki, 84 pp
746 Mazzieri I, Stupazzini M, Guidotti R, Smerzini C (2013) SPEED: Spectral elements in
747 elastodynamics with Discontinuous Galerkin: a non-conforming approach for 3D
748 multi-scale problems. *Int J Numer Meth Eng* 95 (12): 991–1010
749 Panou AA, Hatzidimitriou PM, Theodoulidis N, Stylianidis KC, Triantafyllidis P,·
750 Zacharopoulos S (2014) Comparison of damage data from questionnaires and field
751 survey: the case of the June 20, 1978 Thessaloniki (Northern Greece) M6.5
752 earthquake. *Bull Earthq Eng* 12 (6): 2821–2841
753 Paolucci R, Mazzieri I, Smerzini C, Stupazzini M (2014) Physics-based earthquake ground
754 shaking in large urban areas. *In Perspectives on European Earthquake Engineering*
755 *and Seismology, Second European Conference on Earthquake Engineering and*
756 *Seismology*, Istanbul, vol. 34, chap. 10, pp. 331–359, ed. Ansal, A., Springer.
757 Paolucci R, Mazzieri I, Smerzini C (2015). Anatomy of strong ground motion: near-source
758 records and 3D physics-based numerical simulations of the Mw 6.0 May 29 2012 Po
759 Plain earthquake, Italy. *Geophys J Int* 203: 2001-2020.

760 Paolucci R, Gatti F, Infantino M, Smerzini C, Özcebe AG, Stupazzini M (2017) Broad-band
761 ground motions from 3D physics-based numerical simulations using Artificial Neural
762 Networks, *Bull Seismol Soc Am*, submitted for publication.
763 Papazachos BC, Papazachou C (1997) The Earthquakes of Greece. Ziti Publications,
764 Thessaloniki.
765 Park J, Bazzurro P, Baker JW (2007) Modeling spatial correlation of ground motion intensity
766 measures for regional seismic hazard and portfolio loss estimation. *In: Kanda J,*
767 *Takada T, Furuta H (eds) Applications of statistics and probability in civil*
768 *engineering*. Taylor & Francis, London
769 Penelis G, Sarigiannis D, Stavrakakis E, Stylianidis K (1988) A statistical evaluation of
770 damage to buildings in the Thessaloniki, Greece, Earthquake of June 20, 1978. *In*
771 *Proc. of the 9th world conference on earthquake engineering*, Tokyo-Kyoto, Japan,
772 1988, Vol II, pp 187–192
773 Penelis G (2008) Thessaloniki 1978 earthquake. Turning point in seismic protection of
774 Greece. *In Proc. of 30 years after the Thessaloniki earthquake. Memoirs and*
775 *perspectives*, Aristotle University of Thessaloniki, May 2008 (in Greek).
776 Pitilakis K *et al.* (2004). An advanced approach to earthquake risk scenarios with applications
777 to different European towns: Synthesis of the application to Thessaloniki city. RISK-
778 UE Report, Research Project, European Commission, DG XII2001-2004, CEC:
779 EVK4-CT-2000-00014
780 Pitilakis K, Crowley H, Kaynia A, editors. (2014) SYNER-G: Typology definition and
781 fragility functions for physical elements at seismic risk. *In Series Geotechnical,*
782 *Geological and Earthquake Engineering*, 27. Netherlands: Springer.
783 Pitilakis K, Riga E and Anastasiadis A (2015) New Design Spectra in Eurocode 8 and
784 Preliminary Application to the Seismic Risk of Thessaloniki, Greece. *In Perspectives*
785 *on Earthquake Geotechnical Engineering, Vol. 37 of the series Geotechnical,*
786 *Geological and Earthquake Engineering*, pp 45-91, doi 10.1007/978-3-319-10786-
787 8_3.
788 Porter K, Jones L, Cox D, Goltz J, Hudnut K, Mileti D, Perry S, Ponti D, Reichle M, Rose
789 AZ, Scawthorn CR, Seligson HA, Shoaf KI, Treiman J, Wein A (2011) The ShakeOut

790 Scenario: A Hypothetical Mw7.8 Earthquake on the Southern San Andreas Fault.
791 *Earthq Spectra* 27(2): 239-261
792 Riga E, Karatzetzou A, Mara A, Pitilakis K. (2017) Studying the uncertainties in the seismic
793 risk assessment at urban scale applying the Capacity Spectrum Method: The case of
794 Thessaloniki. *Soil Dyn Earthq Eng* 92: 9–24
795 Robinson D, Fulford G, Dhu T. (2005) EQRM: Geoscience Australia's Earthquake Risk
796 Model. Technical manual version 3.0. Geoscience Australia Record 2005/01.
797 Roumelioti Z, Theodulidis N, Kiratzi A (2007) The 20 June 1978 Thessaloniki (Northern
798 Greece) earthquake revisited: slip distribution and forward modelling of geodetic and
799 seismological observations. *In Proc. of the 4th International Conference on*
800 *Earthquake Geotechnical Engineering*, June 25-28, Paper no. 1594
801 Smerzini C, Galasso C, Iervolino I, Paolucci R (2014). Ground motion record selection based
802 on broadband spectral compatibility. *Earthq Spectra* 30(4): 1427–1448.
803 Smerzini C, Pitilakis K, Hashemi K (2017) Evaluation of earthquake ground motion and site
804 effects in the Thessaloniki urban area by 3D finite-fault numerical simulations. *Bull*
805 *Earthq Eng* 15(3): 787–812
806 Stupazzini M, Infantino M, Allmann A, Kaeser M, Paolucci R, Mazzieri M, Smerzini C
807 (2017) PSHAe (Probabilistic Seismic Hazard Assessment Enhanced): the case of
808 Istanbul. *In Proc. of the 16th World Conference on Earthquake Engineering*
809 *(16WCEE2017)*, Santiago, Chile.
810 Taborda R, Bielak J. (2014) Ground-Motion Simulation and Validation of the 2008 Chino
811 Hills, California, Earthquake Using Different Velocity Models. *Bull Seismol Soc Am*
812 104(4): 1876–1898.
813 Villani M, Faccioli E, Ordaz M, Stupazzini M (2014) High-resolution seismic hazard analysis
814 in a complex geological configuration: the case of the Sulmona basin in Central Italy.
815 *Earthq Spectra* 30(4): 1801–1824.
816 Weatherill GA, Silva V, Crowley H, Bazzurro P (2015) Exploring the impact of spatial
817 correlations and uncertainties for portfolio analysis in probabilistic seismic loss
818 estimation. *Bull Earthq Eng* 13(4):957–981, doi: 10.1007/s10518-015-9730-5